nature methods

Article

https://doi.org/10.1038/s41592-023-02165-7

Multimodal probing of T-cell recognition with hexapod heterostructures

Received: 4 July 2022

Accepted: 26 December 2023

Published online: 19 February 2024

Check for updates

Xiaodan Huang[1,7], Lingyuan Meng[1,7], Guoshuai Cao[1], Aleksander Prominski[2], Yifei Hu[1,3], Chuanwang Yang[4], Min Chen[1], Jiuyun Shi[2], Charles Gallagher[5], Thao Cao[1], Jiping Yue[2], Jun Huang[1] ✉ & Bozhi Tian[2,4,6] ✉

Studies using antigen-presenting systems at the single-cell and ensemble levels can provide complementary insights into T-cell signaling and activation. Although crucial for advancing basic immunology and immunotherapy, there is a notable absence of synthetic material toolkits that examine T cells at both levels, and especially those capable of single-molecule-level manipulation. Here we devise a biomimetic antigen-presenting system (bAPS) for single-cell stimulation and ensemble modulation of T-cell recognition. Our bAPS uses hexapod heterostructures composed of a submicrometer cubic hematite core (α-Fe_2O_3) and nanostructured silica branches with diverse surface modifications. At single-molecule resolution, we show T-cell activation by a single agonist peptide-loaded major histocompatibility complex; distinct T-cell receptor (TCR) responses to structurally similar peptides that differ by only one amino acid; and the superior antigen recognition sensitivity of TCRs compared with that of chimeric antigen receptors (CARs). We also demonstrate how the magnetic field-induced rotation of hexapods amplifies the immune responses in suspended T and CAR-T cells. In addition, we establish our bAPS as a precise and scalable method for identifying stimulatory antigen-specific TCRs at the single-cell level. Thus, our multimodal bAPS represents a unique biointerface tool for investigating T-cell recognition, signaling and function.

T cells, a category of leukocytes, play a central role in mediating cellular immune responses to cancer, infection and autoimmune diseases. T cells use T-cell receptors (TCRs) to recognize antigenic peptides presented by major histocompatibility complexes (pMHCs) on antigen-presenting cells (APCs), which initiates T-cell signaling and associated immune responses. T cells can also be transduced with genetically engineered chimeric antigen receptors (CARs) to recognize tumor-associated antigens (for example, CD19). Upon antigen recognition by TCRs or CARs, T cells proliferate, differentiate and execute effector functions, including cytokine secretion and lysis of target cells[1,2].

Antigen recognition by TCRs and CARs underpins many immunotherapies for the treatment of cancer and/or infection and the prevention of transplant rejection[3–5]. Studies using synthetic or artificial antigen-presenting systems with adjustable design parameters have elucidated TCR molecular structures, conformation, nano-organization, kinetics, segregation and catch bonds during TCR recognition[6–9]. For example, at the ensemble level, commercially

[1]Pritzker School of Molecular Engineering, University of Chicago, Chicago, IL, USA. [2]Department of Chemistry, University of Chicago, Chicago, IL, USA. [3]Pritzker School of Medicine, University of Chicago, Chicago, IL, USA. [4]The James Franck Institute, University of Chicago, Chicago, IL, USA. [5]Department of Physics, University of Chicago, Chicago, IL, USA. [6]The Institute for Biophysical Dynamics, University of Chicago, Chicago, IL, USA. [7]These authors contributed equally: Xiaodan Huang, Lingyuan Meng. ✉e-mail: huangjun@uchicago.edu; btian@uchicago.edu

https://doi.org/10.1038/s41592-023-02165-7

Table 1 | Molecular designs for the hexapod-bAPS across diverse experiments

Hexapod modification	Interfaced cell	Experimental purpose	Results
A2D2 streptavidin and PE-anti-CD19	–	Single-molecule imaging	One single ligand molecule on each tip of a hexapod
None	Primary 5C.C7 CD4$^+$ T cells	Biochemical single-cell micropipette experiments	Poking or force does not induce calcium signal
pMHC (p=MCC)	Primary 5C.C7 CD4$^+$ T cells		Single pMHC induces calcium signal
pMHC (p=MCC, 102S or Null)	Primary 5C.C7 CD4$^+$ T cells		T cell discriminates peptides with only one amino acid mutation
pMHC (p=OVA, G4 or Null)	Primary OT-1 CD8$^+$ T cells		
Anti-CD3 or CD19	CAR-T cells		TCR transduction is more efficient than that of CAR
Anti-CD3 or CD19	T or CAR-T cells	Biointerface scanning electron microscopy imaging	Tight hexapod–cell biointerface
CD19	CAR-T cells	Biointerface confocal imaging	
AF555-streptavidin and CD19	CAR-T cells	FRET	Interaction occurs at the sites of physical connection
AF555-streptavidin and anti-CD45	CAR-T cells		Biological control
pMHC (p=MCC)	Primary 5C.C7 CD4$^+$ T cells	Tracking analysis	No aggregation; directed motion
pMHC (p=OVA or MCC)	Primary CD8$^+$ or CD4$^+$ T cells	Biophysical rotation experiments	Primary T-cell activation was amplified by rotating hexapods
Anti-CD3 or CD19	CAR-T cells		CAR activation was amplified by rotating hexapods
Anti-CD3 and anti-CD28	Primary CD8$^+$ or CD4$^+$ T cells		T-cell activation was amplified by rotating hexapods
pMHC (p=Null), BSA or isotype antibody	T cells or CAR-T cells		Negative controls
Streptavidin	Biotinylated T cells		
pMHC (p=OVA or MCC)	Primary CD8$^+$ or CD4$^+$ T cells	Identify stimulatory antigen-specific TCRs	Stimulatory antigen-specific TCRs identified through hexapods

available Dynabeads are used in T-cell expansion, isolation and cytokine production[10], and scaffolds have facilitated the expansion and manufacturing of T cells with increased efficiency[11]. At the single-cell level, synthetic Janus particles have been used to regulate membrane dynamics, clustering of intracellular proteins, and calcium signaling in T cells[12].

While existing synthetic material approaches to T-cell research primarily focus on the ensemble or single-cell level, the next advance in our understanding of immunology is expected to arise from data at the nanometer scale and single-molecule level. TCR-pMHC recognition is highly specific. Effective T-cell responses rely on highly diverse TCR repertoires for identification of a wide range of antigens, and a comprehensive understanding of TCR or CAR recognition at the single-molecule level is crucial for vaccine development and cellular immunotherapy[13,14]. However, single-molecule studies of TCR and CAR recognition require precise manipulation of the synthetic material, which is currently beyond the scope of most existing artificial APC toolkits. TCRs have been suggested to have greater recognition sensitivity than CARs (albeit without reaching single-molecule resolution)[15,16]; therefore, single-molecule resolution is also essential to gain critical insights into the CAR recognition process. Furthermore, current artificial APCs cannot accurately probe the mechanotransduction of suspension T cells. Recently, single-molecule methods such as those involving nanoarrays[17] and Förster resonance energy transfer (FRET)[18] have contributed to a better understanding of immune cell activation dynamics. However, nanoarrays using prefabricated chips with geometrically arranged molecules on surfaces are mainly designed for sole purpose and can be costly, while FRET requires a donor–acceptor pair <10 nm apart to ensure effective energy transfer, precluding its use in large-scale cellular dynamics studies. New modes of modulation are required to physiologically study the nanoscale physical impact on T cells in vitro with single-molecule resolution.

Identification of stimulatory antigen-specific TCRs is currently the bottleneck in development of TCR-based immunotherapies. Current methods for identifying antigen-specific TCRs, based either on binding (for example, MHC multimers) or function (for example, ELISpot), are limited by low sensitivity, specificity, precision and scalability[19]. For example, MHC tetramers[20] lack the surface structures and mechanical properties of APCs and cannot apply the controllable forces required to effectively stimulate the mechanosensory TCRs and generate physiologically relevant immune responses. Furthermore, high affinity but non-stimulatory TCRs occur frequently in the human T-cell repertoire. Force-mediated catch bonds are required to differentiate between stimulatory and non-stimulatory TCRs with equal affinity[7,21,22]. Conversely, function-based methods are often tedious and labor-intensive[19]. There is a critical need for a high-sensitivity, scalable method that combines the strengths of both the binding- and the function-based methods for precise identification of stimulatory antigen-specific TCRs.

Here, we introduce a biomimetic antigen-presenting system (bAPS) composed of a bifunctional hematite–silica hexapod heterostructure. We demonstrate how the bAPS may be applied to investigate the signaling and biochemical–mechanical dual sensitivity of T cells (Table 1). Using a glass micropipette, the bAPS can be manipulated at the single-cell level with single-molecule resolution via the hexapod branches to probe T-cell biochemical sensitivity (assay 1). The bAPS can be manipulated with rotating magnetic fields via the magnetic hematite core to investigate how magnetic torques mediate T-cell activation and immune responses at the ensemble level with single-cell resolution (assay 2). Furthermore, the bAPS provides a precise and scalable approach to identify stimulatory antigen-specific TCRs at the single-cell level, which is a significant challenge in the field of TCR-based immunotherapy (assay 3).

https://doi.org/10.1038/s41592-023-02165-7

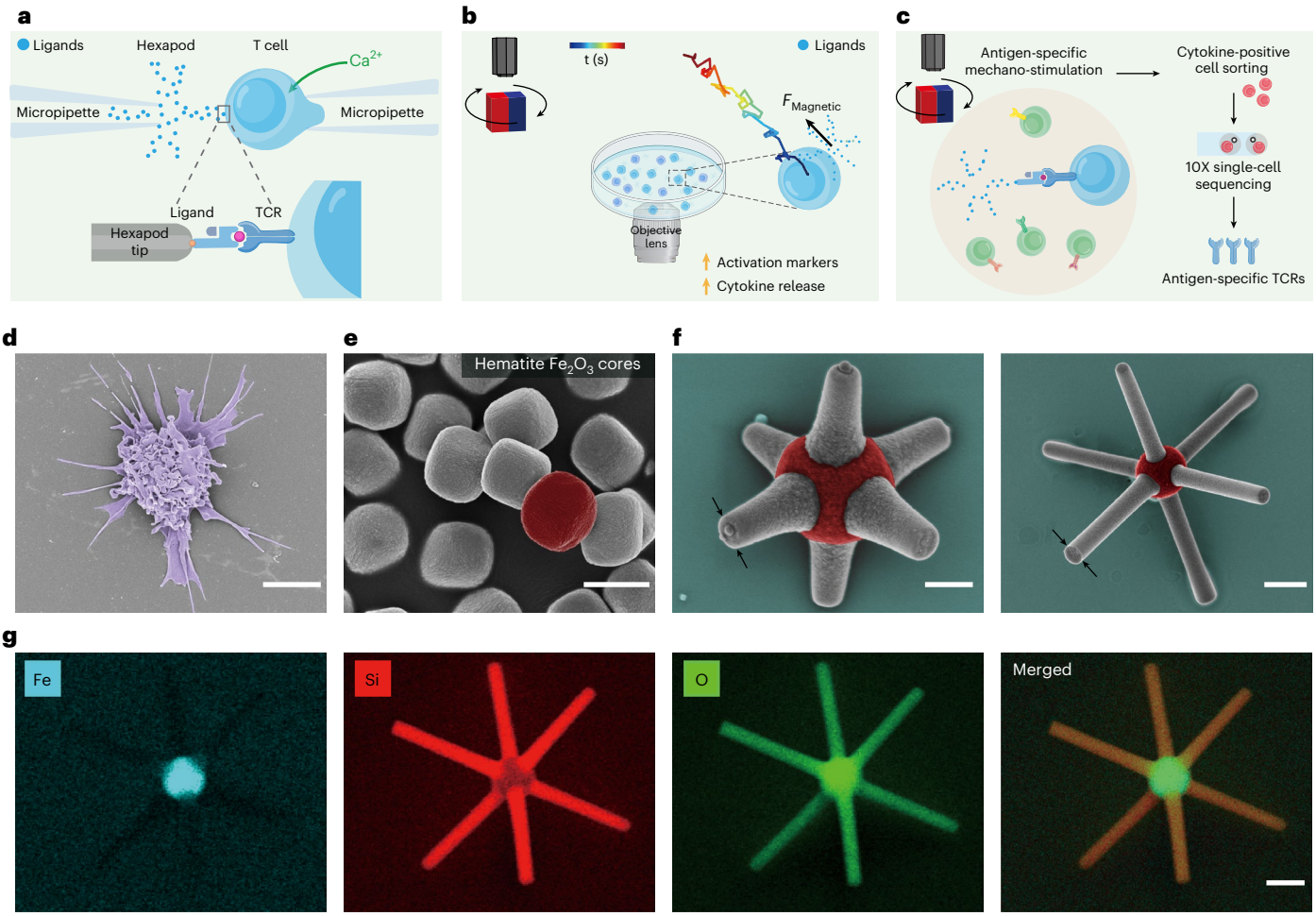

Fig. 1 | Hexapod-enabled molecular level interrogation of T-cell recognition. **a**, Single-molecule investigation of T-cell biochemical sensitivity. The unique hexapod structure enables single-particle manipulation using an open-orifice aspiration micropipette. **b**, Biophysical investigation of T-cell mechanosensitivity. The hematite hexapods can be used for biophysical interrogation of the impact of force on floating T cells. **c**, Identification of antigen-specific TCRs at the single-cell level. The hexapod system can be used for scalable screening of antigen-specific TCRs. **d**, Representative scanning electron microscope (SEM) image of a dendritic cell showing structural similarity to the biomimetic hexapods. The experiment was repeated independently five times with similar results. **e**, Representative SEM image showing the synthesized hematite microcubes. The experiment was repeated independently ten times with similar results. **f**, Synthesized hexapods have a symmetrical structure with six branches, one on each face of the hematite cubes. Branch length can be tuned during synthesis by aging under different temperatures (left, aging at room temperature; right, aging at 37 °C). Branch diameter is 400 nm. The experiment was repeated independently five times with similar results. **g**, Energy-dispersive spectroscopy element mapping of a colloidal hexapod. Iron (Fe) in blue, silicon (Si) in red, oxygen (O) in green and the merged element distribution indicate that a hexapod has six silica branches and an iron oxide core. Scale bars: **d**, 5 µm; **e**, **f** (right) and **g**, 1 µm; **f** (left), 500 nm.

Results

Hexapod heterostructure design and synthesis

We develop a synthetic material system capable of probing T-cell-mediated cellular immunity from the single-cell to the single-molecule level (Fig. 1). Three assay capabilities were considered essential: single-molecule stimulation of T-cell signaling for biochemical investigations (assay 1, Fig. 1a); application of torque in suspension T cells for biophysical investigations (assay 2, Fig. 1b); and precise identification of stimulatory antigen-specific TCRs at the single-cell level (assay 3, Fig. 1c). The biomimetic hexapod heterostructures of the bAPS, featuring a hematite (α-Fe_2O_3) core and six silica branches to mimic the structure of APCs (Fig. 1d), meet all three criteria.

We chose hematite microcubes (length ~860 nm) as the hexapod core due to their weak magnetic properties, which cause less particle aggregation (Fig. 1e,g and Supplementary Table 1). The hematite core facilitates behavior analogous to magnetically controlled micro-robotics[23] by enabling magnetic torque, which directly imparts force onto the TCRs and CARs. The silica branches (diameter ~50–500 nm, length ~1–3 µm) were grown on each face (Fig. 1f,g), resembling dendritic cell and cancer cell microvilli. The branches enable direct bioconjugation of specific antigens and delineate spatial boundaries for the bAPS–T-cell interaction interfaces (Fig. 1f and Supplementary Fig. 1). This architecture enables the bAPS to dynamically engage and activate antigen-specific T cells. The monodispersed hexapods remain stable in PBS or culture medium for more than 24 hours with minimal release of ions (Supplementary Figs. 2–4) and are suitable for in vitro cellular immunology applications.

Biochemical modification and quantification of hexapod surfaces

To investigate biochemical signaling at the single-molecule level in individual T cells, stimulatory or non-stimulatory ligands and proteins were conjugated to the hexapods via streptavidin–biotin interactions, and the modified hexapods dispersed well in PBS (Extended Data Fig. 1, Supplementary Fig. 5 and Table 1). To quantify the coating density, we labeled CD19-conjugated hexapods with phycoerythrin (PE)-anti-CD19 antibody. CD19 density on hexapods was quantified

as 7.54 (microscopy) and 7.87 (flow cytometry) molecules per square micrometer using PE calibration beads (Supplementary Figs. 6 and 7). The nanoscale branch tips (r ~ 200 nm) of hexapod heterostructures spatially confine the hexapod–cell interface to 0.13 μm^2. On average, this area harbors a single ligand molecule (Supplementary Fig. 7). The conjugation dosage was kept the same in all ligand modifications.

To confirm single-molecule presentation at the hexapod tip, we conducted single-molecule imaging experiments using our well-established methods[13]. We coated a biotinylated coverslip with single streptavidin–phycoerythrin (SA-PE) molecules. Meanwhile, we conjugated PE-labeled ligand to the hexapod surface using divalent streptavidin (2 alive subunits and 2 dead subunits, A2D2)[24,25], which ensured monovalent ligand presentation on each hexapod tip (Fig. 2a). We then introduced the PE-labeled hexapods to the same coverslip. The images clearly showed that each hexapod tip contained only a single PE molecule, and statistical analysis fully supported the presence of a single ligand molecule on each tip (Fig. 2b–d). We also used wild-type tetrameric streptavidin (4 alive subunits, A4) and again demonstrated only one single molecule on each hexapod tip (Extended Data Fig. 2).

Single-molecule probing of TCR sensitivity and signaling

TCR-pMHC recognition is highly specific and single-residue alterations on peptides can induce distinct T-cell responses. The symmetrical bAPS can be applied to single-cell, single-molecule biochemical studies using a micropipette. A single silica branch fits into the micropipette orifice, four lateral branches prevent indrawing, and the last branch is for single-molecule probing (Figs. 1a and 2e). To form a confined bAPS–T-cell contact interface, we used a micromanipulator system (Supplementary Fig. 8) in which one micropipette holds a pMHC-coated hexapod and another holds a calcium indicator-labeled primary T cell. We observed calcium fluxes in primary 5C.C7 CD4$^+$ T cells upon contact with hexapods loaded with agonist moth cytochrome c peptide 88-103 (MCC)-bound I-E^k MHC (denoted as MCC-hexapod). However, no calcium signals were detected for unmodified hexapods. We found that TCR signaling is specific to the agonist pMHC, but not to non-specific biophysical contact or poking force (Supplementary Fig. 9).

We next coated the hexapods with a structurally similar pMHC in which the peptide differs by only one amino acid (Supplementary Fig. 10). Single amino acid alterations in the short peptide sequence induced distinct calcium profiles in the interfaced T cell, indicating that the TCRs can differentiate even one amino acid difference on our hexapods. For example, the hexapods loaded with weak agonist G4-bound H-2K^b MHC (denoted as G4-hexapod) induced reduced calcium flux in OT-1 CD8$^+$ T cells when compared to the OVA-hexapods, or hexapods loaded with agonist ovalbumin peptide residues 257-264 (OVA)-bound H-2K^b MHC (Fig. 2f,g and Supplementary Fig. 10). Similarly, the weak agonist 102S-hexapod induced delayed calcium flux with reduced intensity compared with the agonist MCC-hexapod in 5C.C7 CD4$^+$ T cells (Supplementary Figs. 10 and 11). In addition, hexapods with non-stimulatory null peptides did not elicit calcium fluxes in either CD8$^+$ or CD4$^+$ T cells (Fig. 2f,g and Supplementary Figs. 10 and 11).

Altogether, the data suggest that our hexapods can serve as potent artificial APCs for triggering stimulatory antigen-specific T-cell responses. Similar peptides presented on hexapods can be structurally discriminated by the TCRs with a biochemical sensitivity down to the single-amino acid level. These observations align well with previous studies using authentic APCs[13,25–27]. The hexapod-bAPS is a unique synthetic material system capable of probing TCR recognition with single-antigen sensitivity and single-amino acid specificity (beyond the scope of existing artificial APC technologies) and represents a new platform to study signaling and function in immune cells (Supplementary Table 2).

Determining CAR sensitivity by hexapods

CARs are synthetic receptors that consist of an extracellular single-chain antibody fragment (scFv), an extracellular hinge, a transmembrane region, and intracellular signaling domains (Supplementary Fig. 12a,b)[28], and CAR-T cells have achieved remarkable success in the treatment of B-cell malignancies with high levels of CD19$^+$ tumor cells; however, much remains unknown in terms of CAR recognition and signaling.

We next used the hexapod to determine the recognition sensitivity of CAR-T cells to target ligands. We constructed CD19-targeting CAR-T cells, which co-express endogenous TCRs and anti-CD19 CARs (Supplementary Fig. 12c–g). When presented by hexapods, a single anti-CD3 antibody (TCR targeting) induced strong calcium signaling while a single CD19 molecule (CAR targeting) induced negligible calcium signaling in CAR-T cells (Fig. 2h,i and Extended Data Fig. 3). By contrast, NALM-6 cells expressing high-level CD19 induced saturated calcium signals in CAR-T cells (Extended Data Fig. 3). NALM-6 cells and CAR-T cells formed tight interfaces with high CAR density (Supplementary Figs. 13 and 14), indicating that CAR signaling strength is highly dependent on CD19 density. These results, obtained using our bAPS, also indicate that TCRs are significantly more sensitive than the CARs, aligning with previous findings[15,16,29] and providing insight into the limited efficacy of CAR-T cell therapies in treating tumors with low or diminished antigen expression. We envision that the hexapod platform may facilitate large-scale screening for the rational design of next-generation high-sensitivity CARs against solid tumors with antigen downregulation and loss[30].

Magnetic hexapod-induced rotation of suspension T cells

Developing a mechanical force toolkit to investigate the mechanosensing of suspension T cells is challenging due to their free-floating nature. Existing methods to investigate T-cell mechanosensing require immobilization of T cells onto a pre-coated substrate (Supplementary Table 2)[7,31,32], the process of which may change both the cytoskeleton network and the physiological conditions, causing further stress to or mechanical loading on the T cells. Several studies have used magnetic microrobots or particles to move single cells without fixation or immobilization. While responses (calcium signaling, in particular) in individual suspension cells can be observed, mechanosensitive responses are not yet quantified. Conventional magnetic particles have also been used to create an oscillatory environment to enhance T-cell activation[33]. However, due to severe aggregations caused by strong magnetic forces, the evaluation of force on individual cells was almost impossible.

The hematite core of the hexapod is weakly magnetic and can generate exogenous forces without noticeable aggregation in a magnetic field. To study hexapod movement in a rotating magnetic field, we placed the hexapods in PBS solution and positioned a rotating magnet nearby (Fig. 3a). We calculated the rotating magnetic field strength (2.3–5.22 mT) based on our experimental set-up (Supplementary Fig. 15) using a mathematical model[34] (Fig. 3b and Supplementary Video 1) and tracked the moving trajectories of hexapods. Each individual hexapod rotated synchronously in the rotating magnetic field without noticeable aggregation (Fig. 3c and Supplementary Video 2). Upon co-culture of functionalized hexapods with T cells or CAR-T cells, hexapods fastened to the cells and formed tight attachments (Fig. 3d and Supplementary Fig. 16). For example, confocal images showed that CD19 molecules strongly colocalized with anti-CD19 CARs at the contact site with an average Pearson coefficient of ~0.79 (Extended Data Fig. 4). Furthermore, in addition to demonstrating the physical colocalization between CD19 molecules and anti-CD19 CARs, we also validated their interactions at contact sites using FRET analysis (Extended Data Fig. 5).

The tight hexapod–cell junctions enabled the rotating hexapods to drive movement of the cells (Fig. 3e and Supplementary Video 3). We used a simplified mean square displacement (MSD) analysis to evaluate the apparent trajectories. We found that the unbound T cells remained relatively stationary with minimal lateral movement, undergoing Brownian motion or normal diffusion (MSD $\propto D \cdot t^{\alpha}$, exponent

https://doi.org/10.1038/s41592-023-02165-7

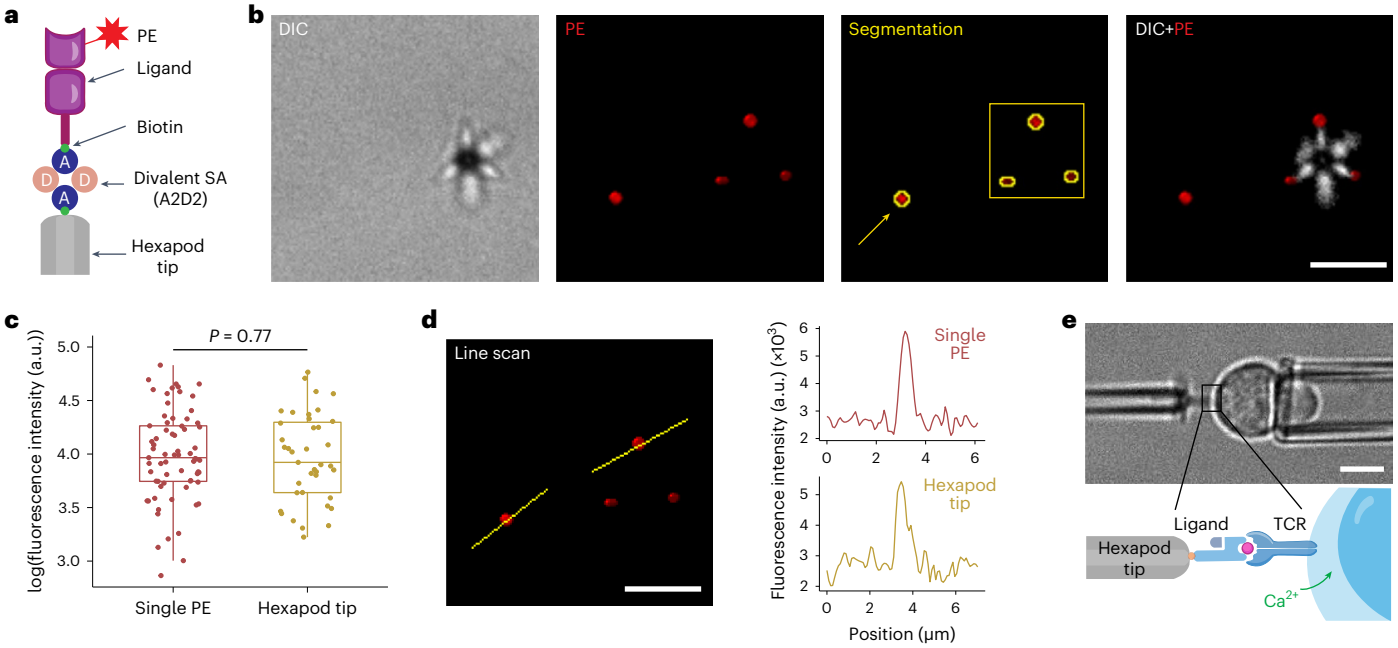

Fig. 2 | Hexapod-based biochemical investigation of T-cell calcium signaling. **a**, Schematic diagram of single ligand presentation by divalent SA (A2D2). **b**, Representative image of PE-conjugated-hexapod and single PE molecules on the coverslip (arrow, single PE molecule; square, hexapod). DIC, differential interference contrast. **c**, Fluorescence intensity comparison between single PE molecules ($n = 69$ independent measurements) and single hexapod tips ($n = 39$ independent measurements) using the Wilcoxon signed-rank test. Box boundaries span the 25th–75th percentiles with the median marked and all the data points from minimum to maximum presented. **d**, Representative fluorescence profiles of a single PE molecule and a hexapod tip. **e**, Representative picture showing the hexapod-bAPS micropipette experiment. **f**, Calcium signal of OT-1 $CD8^+$ T cells stimulated using an OVA-hexapod, a G4-hexapod and a non-stimulatory peptide (Null)-hexapod. **g**, Calcium profiles (mean $F/F_0 \pm$ s.e.m.) were observed upon stimulation with an OVA-hexapod ($n = 13$ independent experiments), G4-hexapod ($n = 9$ independent experiments) or Null-hexapod ($n = 10$ independent experiments). OVA and G4 have only one amino acid difference in their sequence, confirming the amino acid-level biochemical sensitivity of T cells. Right: mean calcium intensity in pMHC-hexapod stimulated cells at each time point (1 frame s^{-1} or $n = 600$ data points). Lines, mean $F/F_0 \pm$ s.d. **h**, Second-generation CAR-T cell calcium response upon stimulation with an anti-CD3-hexapod or a CD19-hexapod. **i**, Anti-CD3-hexapods ($n = 8$ independent experiments for each type of CAR-T cell) induce a stronger calcium flux than the CD19-hexapods ($n = 4$). Data are presented as mean $F/F_0 \pm$ s.e.m. Right: calcium intensity in anti-CD3-hexapod or CD19-hexapod stimulated cells at each time point (1 frame every 2 s or $n = 300$ data points). Lines, mean $F/F_0 \pm$ s.d. Statistical analysis in **g** and **i** was performed using one-way analysis of variance (ANOVA) with Tukey's multiple comparisons. Scale bars, 5 µm.

https://doi.org/10.1038/s41592-023-02165-7

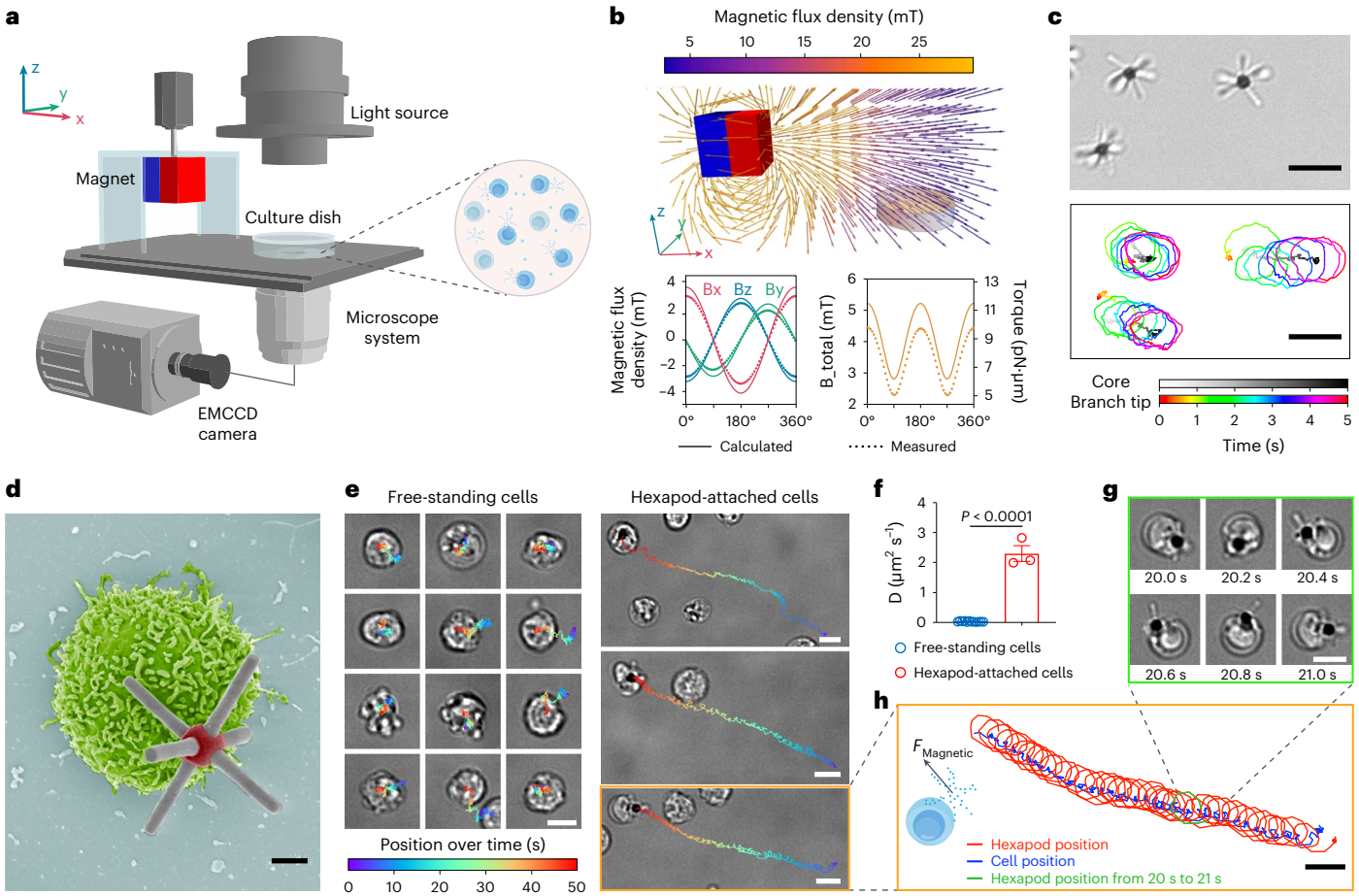

Fig. 3 | Magnetic hexapod-enabled torque on floating T cells. a, Schematic diagram showing the experimental set-up for force quantification. The hexapods are in a cell culture dish at (80 mm, 0, −37.3 mm) relative to a 2.54-cm-cube neodymium (N52) permanent magnet. **b**, Top: calculated magnetic field vectors showing the strength and direction of the field. Bottom: measured and calculated magnetic flux density (field strength) around a hexapod position (center of the cell dish on the lens). Field strength ranges from 2.30 to 5.22 mT, corresponding to 5.06–11.48 pN·μm torques on a hexapod. **c**, Representative image of dispersed hexapods (top) and real-time tracking of single hexapods (bottom) showing periodic rotational motion. The grayscale bar and the rainbow-color bar represent the positions of the hematite core and a hexapod branch tip, respectively. The experiment was repeated independently for five times with similar results. **d**, Representative SEM image showing the tight interaction between a CD19-hexapod and an anti-CD19 CAR-T cell. **e**, Moving trajectories of free-standing T cells and hexapod-attached T cells (MCC-hexapod and 5C.C7 CD4$^+$ T cells). The experiment was repeated independently five times with similar results. **f**, Calculated diffusion coefficient of free-standing T cells ($n = 12$ cells) and hexapod-attached T cells ($n = 3$ cells). Lines, mean F/F$_0$ ± s.e.m. Statistical analysis was performed with the unpaired two-tailed t-test. **g**, Time-lapse pictures showing the positions of a hexapod-attached T cell at several time points (orange box in **e**, green trajectory in **h**). **h**, Tracking trajectories of a hexapod-attached T cell (orange box in **e**). Scale bars: **c**, **e**, **g** and **h**, 5 μm; **d**, 1 μm.

α = 1, where D is the diffusion coefficient and t the elapsed time). In contrast, hexapod-bound cells exhibited hexapod-directed motion (MSD ∝ $D \cdot t^{\alpha}$, α > 1, classic super diffusion due to active transport), with ~250-fold MSD (Supplementary Fig. 17a) compared with the hexapod-free cells.

We estimated the diffusion coefficient from the MSD in a simplified two-dimensional (2D) diffusion approximation and then calculated the speed of suspension T cells with or without hexapod attachment. Hexapod-bound cells had significantly higher diffusion coefficients and velocity than unbound cells (Fig. 3f and Supplementary Fig. 17b). Hexapod-bound cells also displayed turbulent motion (Fig. 3g,h and Supplementary Fig. 17c), which can be attributed to the highly variable magnetic driving force acting on the hexapods. Based on their trajectory, we calculated that a full rotation of hexapod-bound cells took around 1.2 seconds (Supplementary Fig. 17d). This cell rotates at the same speed as the rotating magnetic field, indicating synchronized rotation without time delays (Supplementary Fig. 17e).

Exact determination of instantaneous forces acting on the magnetic hexapods is non-trivial due to the intricate interplay between geometrical and magnetic torques[35], the constantly changing orientation of magnetic moment within the magnetic domain[36], and the ever-evolving fluidic friction or dragging force acting on the moving cells[37]. However, the lack of obvious linear acceleration suggests that hexapod-bound cells are in quasi-equilibrium, achieving a dynamic pseudo-balance between several forces (Fig. 3h). We estimate the torque (τ = m × B) acting on the hexapod using the classical definition of the magnetic moment of the particle $m = I_0 V$, where the spontaneous magnetization per unit volume $I_0 = 2.2 \times 10^3$ A·m^{-1} for hematite[38,39] and the volume of the hematite core $V \approx 1\,\mu m^3$. Therefore, in the magnetic fields used in the experiments (B ≈ 2.30–5.22 mT; Fig. 3b and Supplementary Fig. 18), torque (calculated as $\tau = m \times B$) is 5.06–11.48 pN·μm.

In conclusion, our hexapod differentiates itself from other magnetic force-based assays (Supplementary Table 2). Its unique feature resides in the hematite core, which has comparatively subdued magnetic characteristics, combined with the presence of multiple branch appendages designed for optimized cellular interactions. These properties enable synchronized rotational motion of the individual hexapods, promoting beneficial homogenization of the cell suspension

https://doi.org/10.1038/s41592-023-02165-7

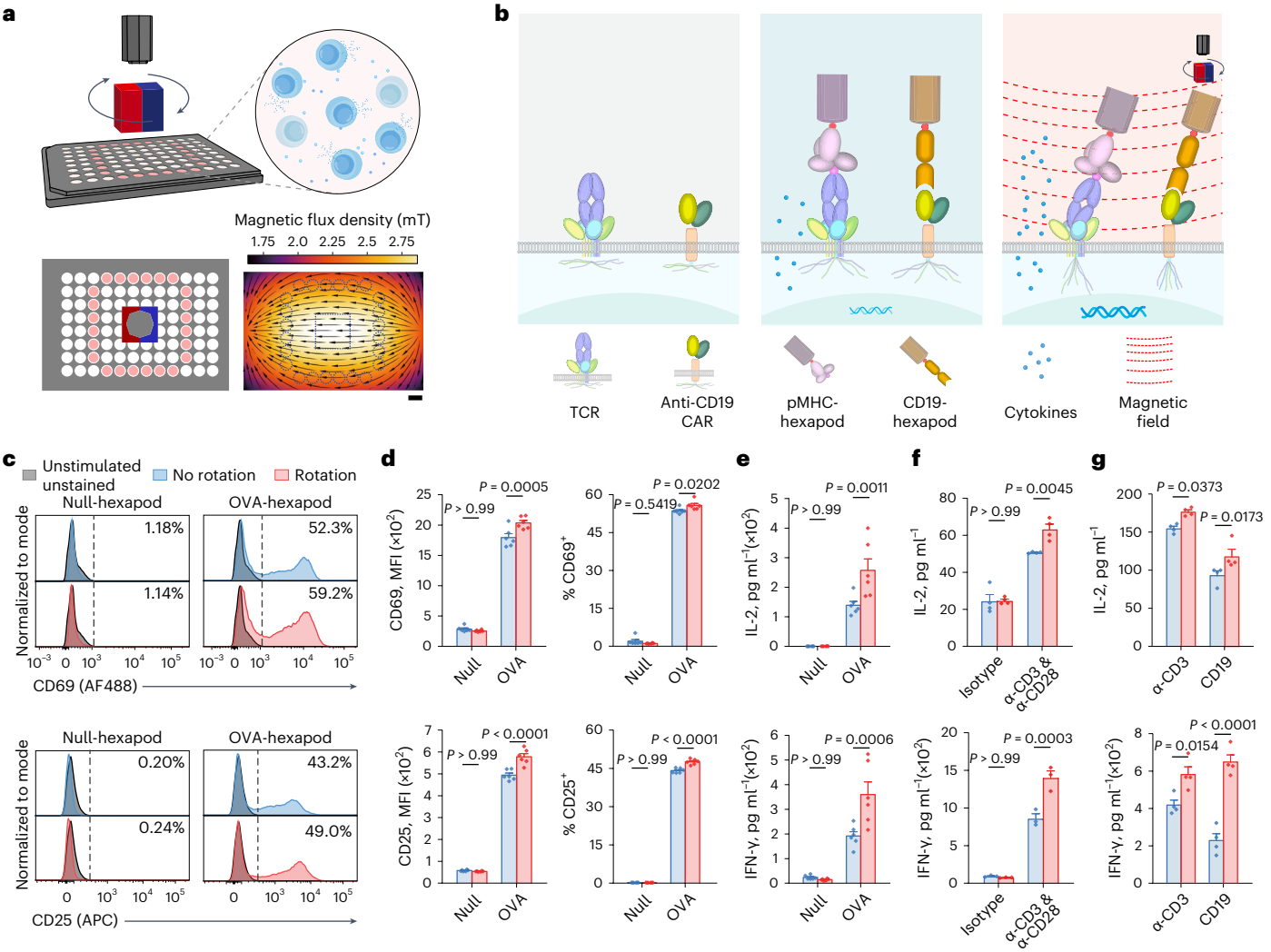

Fig. 4 | Hexapod-bAPS biophysical stimulation of T cells and CAR-T cells. **a**, Schematic diagram showing the experimental set-up for T-cell stimulation using the rotating hexapod-bAPS. Cells were cultured in a 96-well plate. The magnetic field at the plane of the 96-well plate was calculated (color, magnetic flux density; arrows, vectors in the x–y plane). **b**, Schematic diagram showing hexapod biophysical stimulation experiments on floating T cells: left, resting TCR and CAR; middle, activated TCR and CAR; right, activated TCR and CAR under a rotating magnetic field. **c**, Histograms showing representative CD69 (top) and CD25 (bottom) expression in primary OT-1 CD8$^+$ T cells (independent experiment was repeated six times with similar results). Unstimulated cells (in gray) are used for gating. Filled plots indicate co-cultured cells with or without rotation. **d**, Bar graphs of CD69 or CD25 mean fluorescence intensity (MFI) and the percentage of CD69$^+$ or CD25$^+$ cells. CD69 and CD25 expression levels in OT-1 CD8$^+$ T cells ($n = 6$ cultures) were significantly amplified by rotating with OVA-hexapods. **e**, IL-2 and IFN-γ secretion was significantly amplified in hexapod-bAPS rotation-stimulated naive primary mouse CD8$^+$ T cells ($n = 6$ cultures) compared with static hexapod-bAPS-stimulated counterparts. **f**, IL-2 ($n = 4$ independent repeats) and IFN-γ ($n = 3$ independent repeats) secretion was significantly amplified in hexapod-bAPS rotation-stimulated day 6–10 CD8$^+$ T-cell blasts compared with static hexapod-bAPS-stimulated counterparts. **g**, IL-2 ($n = 4$ independent repeats) and IFN-γ ($n = 4$ independent repeats) secretion was significantly increased in rotating anti-CD3- and rotating CD19-hexapod-treated 41BB CAR-T cells compared with static groups, indicating that both the TCR and anti-CD19 CAR are mechanosensitive receptors responsive to hexapod-induced forces. All statistical analysis was performed using one-way ANOVA tests with Bonferroni's multiple comparisons. Data are presented as the individual replicates and the mean ± s.e.m. of multiple independent measurements. Scale bar, 10 mm.

within a rotating magnetic field and, importantly, without obvious cell clumping.

Magnetic force regulation of immune responses in suspension T cells

Mechanical signals, such as shear stress, contact tension and substrate stiffness, contribute to the leukocyte adhesion cascade and regulate T-cell signaling and proliferation[31,40,41]. Although these findings were reported in immobilized T cells, it is highly likely that mechanical cues are also associated with function and activation in suspension T cells in physiological conditions. T cells in the circulatory system are naturally suspension cells (that is, non-adherent T cells). For example, there are more than 10^9 (20–45% of white blood cells) suspension T cells in a liter of human peripheral blood[42]. However, the impact of mechanical forces on the activation of suspension T cells is largely underappreciated.

Studying how suspension T cells respond to mechanical cues (in the present case, torques) will open new areas of fundamental research and hopefully broaden our knowledge of how cells react to their ever-changing environments. Although most T cells and CAR-T cells are usually activated when encountering adhesion cells in non-suspension environments, many other cells or vesicles (for example, circulating tumor cells[43] and exosomes[44] during tumor metastasis or abnormal B cells in blood during leukemia[45]) activate T cells and/or CAR-T cells when they are in suspension. Given these facts, there is growing support

https://doi.org/10.1038/s41592-023-02165-7

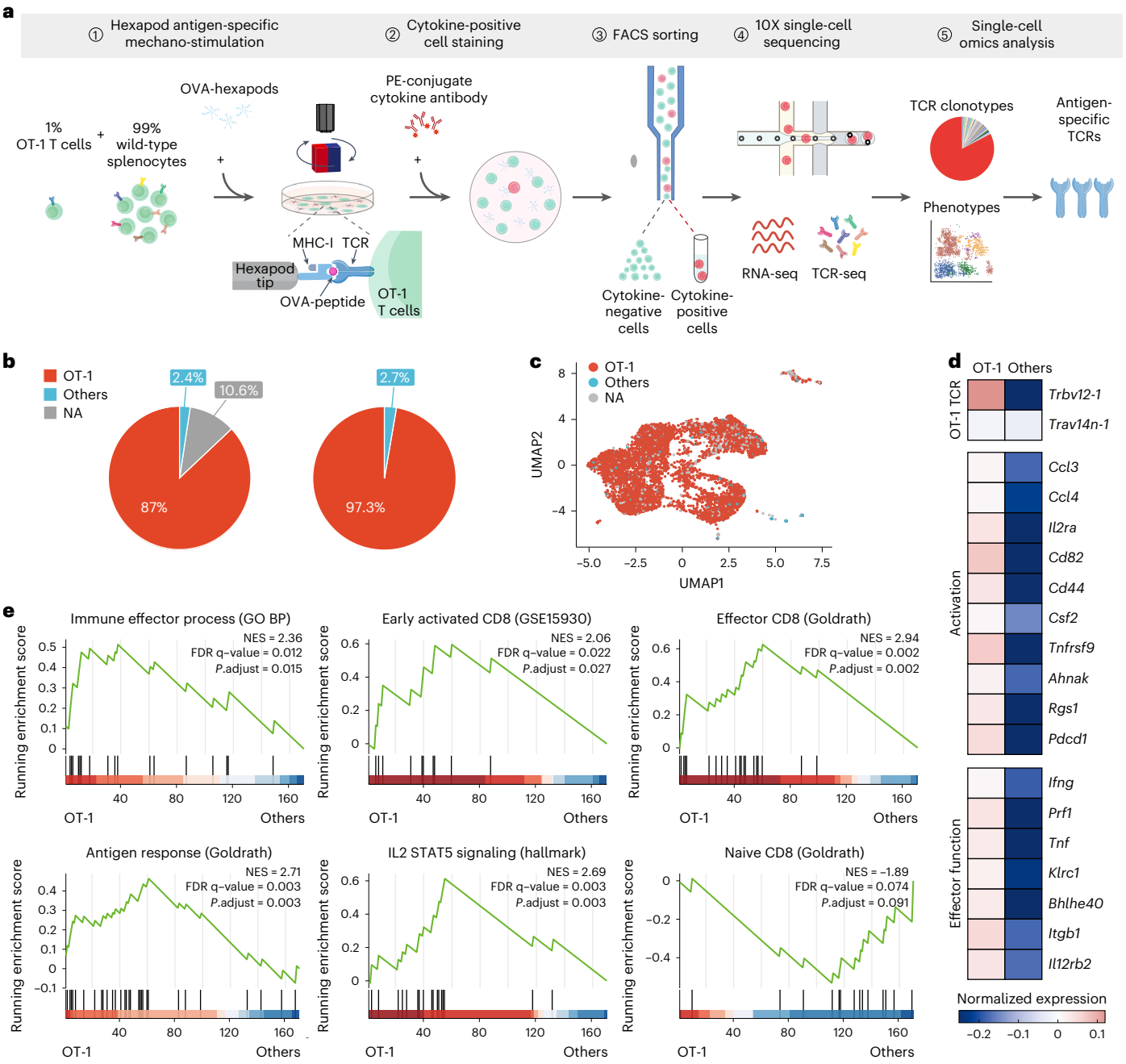

Fig. 5 | Hexapod system enables precise and scalable identification of stimulatory CD8⁺ antigen-specific TCRs at the single-cell level. a, Schematic diagram showing how the hexapod system can be used for precise and scalable screening of antigen-specific TCRs. pMHC-functionalized hexapods are used to stimulate antigen-specific T cells under magnetic torque to produce cytokines. Single cytokine-positive cells are then sorted, sequenced (RNA-seq and TCR-seq), and analyzed to obtain antigen-specific TCRs. MHC-I, major histocompatibility complex class I. **b**, Distribution of clonotype annotations in repertoires, calculated for the entire repertoire (left) or only that with productive TCRs (right). Each cell was classified as either an 'OT-1' T cell (with the corresponding Tcra-V2 and Tcrb-V5 sequence), or 'other' T cell (with other productive TCR sequence), or 'NA' if a cell was captured in the scRNA-seq data without the corresponding TCR information (due to limited depth or dropout). **c**, Uniform manifold approximation and projection (UMAP) showing single cells with corresponding TCR clonotype annotation overlaid in color. **d**, Normalized gene expression of selected genes differentially expressed between OT-1 and other T cells. Group-wise mean expression was calculated as the average scaled gene expression of all cells in that group, and the final values were capped to maximize the dynamic range of the color scale. Genes were grouped into functional categories related to OT-1 cell TCR sequence or function. **e**, GSEA showing selected pathways enriched in OT-1 cells versus Others. A positive enrichment score indicates enrichment in OT-1 cells versus Other cells, and a negative enrichment score indicates enrichment in Other cells versus OT-1 cells. GO BP, Gene Ontology biological process; NES, normalized enrichment score. The *P* value was generated using the permutation test and adjusted for multiple testing using the Benjamini–Hochberg procedure, and the false discovery rate (FDR) was estimated using the FDR q-values.

for the use of suspension synthetic antigen-presenting materials to further investigate the suspension T-cell activation mechanisms[12,46,47].

Having demonstrated that the hexapods can drive T-cell movement through magnetic torque (Fig. 3), we next investigated whether exogenous forces affect immune responses of suspension T cells and CAR-T cells using hexapods. Hexapods were functionalized with stimulatory pMHC or non-stimulatory control molecules and co-cultured with primary mouse transgenic CD8⁺ or CD4⁺ T cells in

the absence or presence of a rotating magnetic field. The magnetic field strength of 2.13–3.07 mT corresponded to torques ranging from 4.69 to 6.75 pN·µm on the hexapod hematite core (Fig. 4a,b and Supplementary Fig. 18).

After a 24-hour incubation, agonist pMHC-functionalized hexapods upregulated expression of CD69 (an early activation marker) and CD25 (a late activation marker) and elevated interleukin-2 (IL-2), tumor necrosis factor (TNF)-α or interferon (IFN)-γ cytokine production in both $CD8^+$ OT-1 T cells (Fig. 4c–f and Supplementary Fig. 19) and $CD4^+$ 5C.C7 T cells (Extended Data Fig. 6). Notably, the rotating magnetic field further upregulated activation marker expression and cytokine production in pMHC-hexapod cells, compared with non-rotating pMHC-hexapod cells (Fig. 4c–f and Extended Data Fig. 6). This indicates that TCRs are mechanosensitive and that hexapod-based rotational motion can amplify T-cell activation and cytokine production.

After stimulation with pMHC-functionalized hexapods and a rotating magnetic field, cell viabilities altered no more than 10% compared with the cell-only (no hexapods) control and were maintained above 80% (Supplementary Fig. 20 and Supplementary Table 3). Our observations indicate a minor reduction in cell viability when co-cultured with stimulatory hexapods (for example, OVA-hexapods) compared with non-stimulatory counterparts. We postulate that this might be due to activation-induced cell death, which would account for the slight dip in viability. Importantly, despite this minor effect, the overall biocompatibility of the hexapod stimulation remains high.

We further tested the effect of hexapod rotation on CAR-T-cell activation. Anti-human-CD3-hexapods or CD19-hexapods were incubated with second-generation 4-1BB CAR-transduced primary human T cells for 24 hours with or without rotating magnetic fields. Consistently, rotating magnetic fields promoted cytokine production in human CAR-T cells incubated with either anti-CD3-hexapods or CD19-hexapods (Fig. 4g), indicating that the CAR is also a mechanosensor.

Due to the dynamic cell–hexapod interactions and the high receptor density at the cell–hexapod interface (Supplementary Fig. 13), the force on a single bond exerted on the TCR or CAR could not be quantified. However, the mechanical impact exerted on the cells can be estimated by the torque, which is dependent on the magnetic field strength and the hexapod dimension. Biotinylated T cells co-cultured with streptavidin-hexapods (no ligands) served as a negative control. No activation markers were elevated, indicating that fluid shear stresses do not activate the T cells (Extended Data Fig. 7). The data suggest that T-cell activation is mediated by specific receptor–ligand interactions.

Altogether, these results demonstrate the application of the hexapods to biophysical modulation studies of T cells and CAR-T cells in suspension. Rotating hexapods can influence receptor activation dynamics, signal transduction and immune function of T cells in suspension. Both TCRs and CARs are responsive to piconewton·micrometer-level torque. Unlike other biophysical tools for studying mechanosensitivity (Supplementary Table 2), our hexapod triggers T-cell signaling and amplifies T-cell activation at the cellular ensemble level in suspension T cells without the need for immobilization.

Precise identification of stimulatory antigen-specific TCRs at the single-cell level

To demonstrate that our hexapods can reliably identify stimulatory antigen-specific TCRs, a low percentage (1%) of OT-1 TCR transgenic $CD8^+$ T cells (with a known αβ TCR sequence) were spiked into a wild-type mouse splenocyte repertoire (with 10^{14}–10^{20} possible αβ TCR suquences[48,49]). The mixture was exposed to hexapods functionalized with OVA–H-$2K^b$ and magnetic force was applied, which caused the hexapods to search for, collide and interact with antigen-specific OT-1 $CD8^+$ T cells. The specific TCR–pMHC interaction led to T-cell activation and production of cytokines (for example, TNF-α and IL-2). Given that cytokine production is a key functional readout of T-cell immune function, antigen-specific T cells can be reliably identified by cytokine production. The cytokine-positive T cells were sorted for single-cell paired TCR and RNA sequencing. The TCR sequencing (TCR-seq) was used to identify antigen-specific TCRs while RNA sequencing (RNA-seq) was used to confirm antigen-specific activation (Fig. 5a). Out of the 89.4% of productive TCRs (10.6% was lost due to limited depth or dropout), 97.3% of the TNF-α-positive cells were OT-1 cells (Fig. 5b,c), indicating that the hexapods successfully targeted the stimulatory antigen-specific T cells. These cells had unique transcriptional signatures compared with the 2.7% of non-OT-1 TNF-α-positive T cells ('Others'), with upregulation of genes related to $CD8^+$ T-cell activation and effector function (Fig. 5d). Furthermore, gene set enrichment analysis (GSEA) confirmed enriched signatures of early T-cell activation and activation-associated effector function rewiring in the OT-1 $CD8^+$ T cells (Fig. 5e).

As previously mentioned, the vast diversity of TCRs in real-world scenarios amounts to trillions of variations. This high degree of diversity can pose challenges when attempting to identify and isolate rare antigen-specific cells. To improve the efficiency of the identification process, we used enrichment techniques (Supplementary Fig. 21a). This led to a significant increase in the prevalence of cytokine-positive cells, from 0.11% in the initial stained mixture to 30.3% in the column elution (Supplementary Fig. 21b–d). This denotes a nearly 300-fold surge in the frequency of cytokine-positive T cells, thereby significantly enhancing the efficiency of subsequent sorting and sequencing procedures for the detection of stimulatory antigen-specific TCRs.

Our new strategy for identifying antigen-specific TCRs using hexapods is highly flexible and can be easily extended to different antigens and cytokines. We validated this method using 5C.C7 $CD4^+$ T cells and MCC–I-E^k functionalized hexapods (Extended Data Fig. 8). Our findings demonstrate the effectiveness, reliability, precision and scalability of the hexapods in identifying stimulatory antigen-specific TCRs.

Discussion

In this study we have developed a material-based bAPS to meet the single-molecule manipulation challenge and study the biochemical and biophysical activation of floating T cells. The bifunctional biomimetic bAPS enables single-molecule stimulation of T-cell signaling for biochemical investigations (assay 1), enables functional studies of T-cell mechanotransduction in suspension (assay 2), and provides a precise and scalable approach for identifying stimulatory antigen-specific TCRs at the single-cell level (assay 3).

We investigate T-cell responses across a spectrum of spatial–temporal, biochemical and mechano-activation studies. Using the micropipette single-cell-signaling assay, we demonstrate how our bAPS probes TCR recognition with single-antigen sensitivity and single-amino acid specificity. The bAPS can also be used to investigate CAR-T cells and has elucidated the insufficient sensitivity of current first- and second-generation CARs. It is expected to serve as a method to examine the recognition sensitivity of future CARs. Furthermore, as a method, the bAPS provides a platform to identify stimulatory antigen-specific TCRs and offers a tool to mechanically modulate T-cell responses. Although the current bAPS is mainly designed for in vitro applications, it can be further developed to detect, measure and manipulate T-cell recognition with good biocompatibility and high throughput in vivo. This material-based biochemical and biophysical investigative approach not only provides insights into TCR and CAR recognition but also fulfills outstanding technological needs in identifying stimulatory antigen-specific TCRs and high-sensitivity CARs, which may catalyze future development of TCR- and CAR-based immunotherapies for cancer, infection and autoimmune diseases.

Materials availability

Reasonable amounts of biological materials used in this study can be obtained from the corresponding authors upon request or from the commercial source stated in the article.

Reporting summary

Further information on research design is available in the Nature Portfolio Reporting Summary linked to this article.

Online content

Any methods, additional references, Nature Portfolio reporting summaries, source data, extended data, supplementary information, acknowledgements, peer review information; details of author contributions and competing interests; and statements of data and code availability are available at https://doi.org/10.1038/s41592-023-02165-7.

References

1. Neal, L. R. et al. The basics of artificial antigen presenting cells in T cell-based cancer immunotherapies. *J. Immunol. Res. Ther.* **2**, 68–79 (2017).
2. Alam, S. M. et al. T-cell-receptor affinity and thymocyte positive selection. *Nature* **381**, 616–620 (1996).
3. Karlsson, A. C., Humbert, M. & Buggert, M. The known unknowns of T cell immunity to COVID-19. *Sci. Immunol.* **5**, eabe8063 (2020).
4. Rurik, J. G. et al. CAR T cells produced in vivo to treat cardiac injury. *Science* **375**, 91–96 (2022).
5. Super, M. et al. Biomaterial vaccines capturing pathogen-associated molecular patterns protect against bacterial infections and septic shock. *Nat. Biomed. Eng.* **6**, 8–18 (2022).
6. van der Merwe, P. A. & Dushek, O. Mechanisms for T cell receptor triggering. *Nat. Rev. Immunol.* **11**, 47–55 (2011).
7. Liu, B., Chen, W., Evavold, B. D. & Zhu, C. Accumulation of dynamic catch bonds between TCR and agonist peptide-MHC triggers T cell signaling. *Cell* **157**, 357–368 (2014).
8. Kobayashi, E. et al. Rapid cloning of antigen-specific T-cell receptors by leveraging the cis activation of T cells. *Nat. Biomed. Eng.* **6**, 806–818 (2022).
9. Steenblock, E. R. & Fahmy, T. M. A comprehensive platform for ex vivo T-cell expansion based on biodegradable polymeric artificial antigen-presenting cells. *Mol. Ther.* **16**, 765–772 (2008).
10. Neurauter, A. A. et al. Cell isolation and expansion using Dynabeads. *Adv. Biochem. Eng. Biotechnol.* **106**, 41–73 (2007).
11. Cheung, A. S., Zhang, D. K. Y., Koshy, S. T. & Mooney, D. J. Scaffolds that mimic antigen-presenting cells enable ex vivo expansion of primary T cells. *Nat. Biotechnol.* **36**, 160–169 (2018).
12. Chen, B. et al. Janus particles as artificial antigen-presenting cells for T cell activation. *ACS Appl. Mater. Interfaces* **6**, 18435–18439 (2014).
13. Huang, J. et al. A single peptide-major histocompatibility complex ligand triggers digital cytokine secretion in CD4(+) T cells. *Immunity* **39**, 846–857 (2013).
14. Irvine, D. J., Purbhoo, M. A., Krogsgaard, M. & Davis, M. M. Direct observation of ligand recognition by T cells. *Nature* **419**, 845–849 (2002).
15. Gudipati, V. et al. Inefficient CAR-proximal signaling blunts antigen sensitivity. *Nat. Immunol.* **21**, 848–856 (2020).
16. Hu, Y. et al. Antigen multimers: specific, sensitive, precise, and multifunctional high-avidity CAR-staining reagents. *Matter* **4**, 3917–3940 (2021).
17. Elnathan, R. et al. Biointerface design for vertical nanoprobes. *Nat. Rev. Mater.* **7**, 953–973 (2022).
18. Žal, T., Žal, M. A. & Gascoigne, N. R. J. Inhibition of T cell receptor–coreceptor interactions by antagonist ligands visualized by live FRET imaging of the T-hybridoma immunological synapse. *Immunity* **16**, 521–534 (2002).
19. Joglekar, A. V. & Li, G. T cell antigen discovery. *Nat. Methods* **18**, 873–880 (2021).
20. Altman, J. D. et al. Phenotypic analysis of antigen-specific T lymphocytes. *Science* **274**, 94–96 (1996).
21. Zhao, X. et al. Tuning T cell receptor sensitivity through catch bond engineering. *Science* **376**, eabl5282 (2022).
22. Sibener, L. V. et al. Isolation of a structural mechanism for uncoupling T cell receptor signaling from peptide-MHC binding. *Cell* **174**, 672–687 (2018).
23. Xie, H. et al. Reconfigurable magnetic microrobot swarm: multimode transformation, locomotion, and manipulation. *Sci. Robot.* **4**, eaav8006 (2019).
24. Howarth, M. et al. A monovalent streptavidin with a single femtomolar biotin binding site. *Nat. Methods* **3**, 267–273 (2006).
25. Huang, J. et al. The kinetics of two-dimensional TCR and pMHC interactions determine T-cell responsiveness. *Nature* **464**, 932–936 (2010).
26. Sasmal, D. K. et al. TCR–pMHC bond conformation controls TCR ligand discrimination. *Cell. Mol. Immunol.* **17**, 203–217 (2020).
27. Rosenberg, J., Cao, G., Borja-Prieto, F. & Huang, J. Lattice light-sheet microscopy multi-dimensional analyses (LaMDA) of T-cell receptor dynamics predict T-cell signaling states. *Cell Syst.* **10**, 433–444.e5 (2020).
28. Weinkove, R., George, P., Dasyam, N. & McLellan, A. D. Selecting costimulatory domains for chimeric antigen receptors: functional and clinical considerations. *Clin. Transl. Immunology* **8**, e1049 (2019).
29. Salter, A. I. et al. Comparative analysis of TCR and CAR signaling informs CAR designs with superior antigen sensitivity and in vivo function. *Sci. Signal.* **14**, eabe2606 (2021).
30. Marofi, F. et al. CAR T cells in solid tumors: challenges and opportunities. *Stem Cell Res. Ther.* **12**, 81 (2021).
31. Zhu, C., Chen, W., Lou, J., Rittase, W. & Li, K. Mechanosensing through immunoreceptors. *Nat. Immunol.* **20**, 1269–1278 (2019).
32. Hu, K. H. & Butte, M. J. T cell activation requires force generation. *J. Cell Biol.* **213**, 535–542 (2016).
33. Majedi, F. S. et al. Augmentation of T-cell activation by oscillatory forces and engineered antigen-presenting cells. *Nano Lett.* **19**, 6945–6954 (2019).
34. Engel-Herbert, R. & Hesjedal, T. Calculation of the magnetic stray field of a uniaxial magnetic domain. *J. Appl. Phys.* **97**, 074504 (2005).
35. Erokhin, S. & Berkov, D. Mechanical orientation of fine magnetic particles in powders by an external magnetic field: simulation-based optimization. *Phys. Status Solidi B* **257**, 2000404 (2020).
36. Abrikosov, A. I., Sacanna, S., Philipse, A. P. & Linse, P. Self-assembly of spherical colloidal particles with off-centered magnetic dipoles. *Soft Matter* **9**, 8904–8913 (2013).
37. Tanimoto, H., Sallé, J., Dodin, L. & Minc, N. Physical forces determining the persistency and centering precision of microtubule asters. *Nat. Phys* **14**, 848–854 (2018).
38. Sacanna, S., Rossi, L. & Pine, D. J. Magnetic click colloidal assembly. *J. Am. Chem. Soc.* **134**, 6112–6115 (2012).
39. Lowrie, W. *Fundamentals of Geophysics* (Cambridge Univ. Press, 2007).
40. Ley, K., Laudanna, C., Cybulsky, M. I. & Nourshargh, S. Getting to the site of inflammation: the leukocyte adhesion cascade updated. *Nat. Rev. Immunol.* **7**, 678–689 (2007).
41. Rossy, J., Laufer, J. M. & Legler, D. F. Role of mechanotransduction and tension in T cell function. *Front. Immunol.* **9**, 2638 (2018).
42. Blumenreich, M. S. in *Clinical Methods: The History, Physical, and Laboratory Examinations* (eds. Walker, H. K. et al.) Ch. 153 (Butterworths, 1990).
43. Pantel, K. & Speicher, M. R. The biology of circulating tumor cells. *Oncogene* **35**, 1216–1224 (2016).
44. Thery, C. et al. Indirect activation of naive CD4(+) T cells by dendritic cell-derived exosomes. *Nat. Immunol.* **3**, 1156–1162 (2002).

45. Terwilliger, T. & Abdul-Hay, M. Acute lymphoblastic leukemia: a comprehensive review and 2017 update. *Blood Cancer J.* **7**, e577 (2017).
46. Hickey, J. W. et al. Efficient magnetic enrichment of antigen-specific T cells by engineering particle properties. *Biomaterials* **187**, 105–116 (2018).
47. Oelke, M. et al. Ex vivo induction and expansion of antigen-specific cytotoxic T cells by HLA-Ig–coated artificial antigen-presenting cells. *Nat. Med.* **9**, 619–625 (2003).
48. Zarnitsyna, V. I., Evavold, B. D., Schoettle, L. N., Blattman, J. N. & Antia, R. Estimating the diversity, completeness, and cross-reactivity of the T cell repertoire. *Front. Immunol.* **4**, 485 (2013).
49. Davis, M. & Bjorkman, P. T-cell antigen receptor genes and T-cell recognition. *Nature* **334**, 395–402 (1988).

Methods

Mice

Our research complies with all relevant ethics regulations. All animal experiments were conducted in accordance with the guidelines of the Institutional Animal Care and Use Committee (IACUC) of the University of Chicago. The study was approved by the IACUC of the University of Chicago. Our study was conducted in accordance with the National Institutes of Health Guide for the Care and Use of Laboratory Animals. All of the mice were bred and maintained in the animal facility of the University of Chicago with an animal protocol approved by the IACUC of the University of Chicago. Mice aged 6–8 weeks were used in this study. Animals of both sexes were used, and the influence of sex was not considered in the data analysis. Mouse rooms and cages were kept at a temperature range of 20–24 °C. The relative humidity was kept at 45–65%.

The 5C.C7 TCR transgenic RAG2 knockout mice with a B10.A background were a generous gift from the National Institute of Allergy and Infectious Diseases (NIAID). The CD45.1 homozygous OT-1 TCR transgenic Tcra-V2 and Tcrb-V5 insert mice with a C57BL/6 background were a generous gift from the Swartz Lab (Pritzker School of Molecular Engineering, University of Chicago). Immune-competent C57BL/6J mice were ordered from the Jackson Laboratory (cat. no. 000664).

Hexapod synthesis

Hexapods were synthesized following a two-step process[50], which includes core synthesis via ferric hydroxide gel condensation and silica branch growth via hydrolysis and condensation from six emulsion droplets, one on each face of the cubic hematite core. First, hematite cubic cores were prepared by thoroughly mixing 10 ml deionized water, 100 ml 2 M $FeCl_3$ solution, and 90 ml 6 M sodium hydroxide solution. The mixture was aged in a 100 °C oven for 8 days in a sealed Pyrex bottle and as-synthesized hematite cubes were washed three times using ethanol by sedimentation and resuspension before drying at 60 °C.

To grow the silica branches, 1 ml anhydrous ethanol, 200 µl deionized water, 200 µl hematite microcube water suspension (1.6 wt%), 100 µl 0.18 M sodium citrate aqueous solution, 200 µl ammonia (28 wt% in water) and 100 µl silica precursor, tetraethoxysilane (TEOS), were introduced in sequence into a 10 ml 1-pentanol with 10% wt/v polyvinylpyrrolidone (molecular weight 40,000) solution. All ingredients were mixed by stirring or shaking by hand, and the mixture was aged in a sealed bottle for 12 hours. Then, reddish powders were washed three times using ethanol and collected by centrifugation at 400 ×*g* for 5 min. A stock solution of hexapods was prepared by adding 1 ml ethanol to the above sedimentation (~6×10^8 particles ml^{-1}). The hexapods can be stored in ethanol in 4 °C for a few months. Hexapod synthesis steps are shown in Extended Data Fig. 1.

Hexapod surface functionalization

Hexapods (150 µl from stock solution) were incubated with 6% (v/v) (3-aminopropyl) triethoxysilane (APTES) in ethanol for 30 min for amino group modification. For biotinylation, washed hexapods were re-dispersed in 450 µl 0.1 M sodium bicarbonate ($NaHCO_3$, pH 8.2) buffer solution, and 50 µl 0.01 M sulfobiotin-NHS (Calbiochem, 203118, freshly prepared in deionized water) was added to make a 1 mM biotin coating environment. Biotinylation was conducted at room temperature (20–23 °C) for 30 min and the hexapods were washed in PBS three times. The washed hexapods were collected using centrifugation and re-dispersed in 400 µl PBS. Then streptavidin (2 mg ml^{-1}) was added to the biotinylated hexapods 1:1 (v/v) for 30 min at 4 °C. Streptavidin-modified hexapods were then blocked with 1% bovine serum albumin (BSA) before incubation with biotinylated pMHC monomers. Hexapods were centrifuged at 400 ×*g* and washed in PBS three times between each step. After the last wash, the modified hexapods were stored at 4 °C ready for use. The functionalization steps are shown in Extended Data Fig. 1.

Biotinylated molecules (pMHCs, CD19, anti-CD3 and anti-CD28)

Biotinylated pMHC monomers were generated at the NIH Tetramer Core Facility. Biotinylated class I H-$2K^b$ MHC was complexed with SIINFEKL (OVA), SIIGFEKL (G4) or RGYVYQGL (VSV, null) peptide. Biotinylated class II I-E^k MHC was covalently complexed with ANERADLIAYLKQATK (MCC), ANERADLIAYLKQASK (102S) or PVSKMRMATPLLMQA (human CLIP 87–101, null) peptide. The biotinylated pMHC monomers and biotinylated human CD19 (ACROBiosystems, CD9-H82E9) were aliquoted and stored at −80 °C and a fresh aliquot was used in each experiment. Biotin anti-mouse CD3ε (clone 145-2C11, BioLegend, 100304), biotin Armenian hamster IgG isotype (clone HTK888, BioLegend, 400904), biotin anti-mouse CD28 (clone 37.51, BioLegend, 102104), biotin Syrian hamster IgG isotype (clone SHG-1, BioLegend, 402004), biotin anti-human CD3 (clone OKT3, BioLegend, 317320), biotin mouse IgG2a, κ isotype (clone MOPC-173, BioLegend, 400204) and biotinylated BSA (BioVision, 7097-5) were stored at 4 °C prior to use.

For surface functionalization, biotinylated pMHC monomer (class I peptide-H-$2K^b$, 0.2 mg ml^{-1}; class II peptide-I-E^k, 0.18 mg ml^{-1}), biotinylated CD19 (ACROBiosystems, 20 µg ml^{-1}), biotinylated anti-mouse CD3ε (BioLegend, 20 µg ml^{-1}) and biotinylated anti-mouse CD28 (BioLegend, 5 µg ml^{-1}) antibodies, biotin Armenian hamster IgG isotype (BioLegend, 20 µg ml^{-1}) and biotin Syrian hamster IgG isotype (BioLegend, 5 µg ml^{-1}), biotinylated anti-human CD3 (BioLegend, 20 µg ml^{-1}), or biotin mouse IgG2a, κ isotype (BioLegend, 20 µg ml^{-1}) were added to streptavidin-modified hexapods. For co-coating with both anti-mouse CD3 and anti-mouse CD28, the molar ratio was controlled to 2:1 (anti-mouse CD3/anti-mouse CD28).

Surface protein quantification

Hexapod surface protein modification was verified with AF488-anti-CD19 (HIB19, BioLegend, 302219) and CD19-hexapods (Supplementary Fig. 5b and Supplementary Video 4). For quantification, PE-anti-human CD19 antibody (HIB19, BioLegend, 302207) was used to label CD19-hexapod and NALM-6 cells. NALM-6 cells were cultured in RPMI 1640 with 10% fetal bovine serum (X&Y Cell Culture, FBS-500), and CD19-hexapods were stored in 1× PBS prior to PE labeling. PE-anti-CD19 labeling was performed under 37 °C for 30 min. Surface protein density was quantified using BD Quantibrite PE beads (BD, 340495, LOT 61567), which have four PE density levels, as the reference. BD Quantibrite PE beads were reconstituted using 0.5 ml 1× PBS with sodium azide plus 0.5% BSA. Optical imaging (Nikon Eclipse Ti2 inverted microscope, ×60 oil immersion objective, numerical aperture (NA) 1.40, pco.panda sCMOS camera, Supplementary Fig. 6) and flow cytometry (BD LSRFortessa Cell Analyzer, Supplementary Figs. 7 and 14) were independently performed to quantify the fluorescence levels on PE-anti-CD19-labeled CD19-hexapods and NALM-6 cells. The BD Quantibrite PE beads were used with PE-labeled CD19-hexapod bAPS and NALM-6 cells in their optimized instrument settings.

Cells

To obtain mouse T cells, 5C.C7 or OT-1 mouse spleen was collected and run through a 70-µm cell strainer with warm complete medium, that is, RPMI 1640 with L-glutamine medium (Cytiva, SH30027.01) containing 10% FBS (X&Y Cell Culture, FBS-500) and supplemented to a final concentration with 1% Penicillin–Streptomycin (Life Technologies, 15140122_3683884612) and 50 µM β-mercaptoethanol (Sigma-Aldrich, M3148).

Splenocytes were resuspended in 5 ml RBC Lysis Buffer (Life Technologies, 00-4300-54) for 5 min, washed three times, and resuspended in 5 ml complete medium. A total of 10 µM MCC peptide (amino acids 88–103, ANERADLIAYLKQATK) or 10 nM OVA peptide (amino acids 257–264, SIINFEKL) was added to stimulate T-cell proliferation on day 0, and 100 U ml^{-1} recombinant mouse IL-2 (Sigma-Aldrich, I0523) was

added the following day. Naive T cells were used for the cell surface marker test and cytokine production evaluation; day 6–10 T-cell blasts were used for the cytokines and calcium tests. Live T-cell suspensions were separated from the dead cells using Ficoll-Paque Plus density gradient media (GE Healthcare, 17-1440-02) and density gradient centrifugation (centrifuged at 400 ×*g* for 10 min at 4 °C, acceleration/deceleration SLOW/SLOW). $CD4^+$/$CD8^+$ T cells were then collected by negative selection with the MojoSort Mouse $CD4^+$/$CD8^+$ T-cell Isolation Kits (BioLegend, 480033, 480035). After three washes, cells were resuspended in the complete medium for use.

NALM-6 cells were a generous gift from J. Rowley (purchased from DSMZ, cat. no. ACC128). E6-1 Jurkat cells were a generous gift from H. Schreiber (purchased from ATCC, cat. no. TIB-152). 293T cell line for lentiviral packaging was purchased from Takara Clontech (632180).

2D fluorescent micropipette assays

A single-cell micropipette set-up was used to investigate the biochemical impact of single hexapod stimulation on an individual cell, with calcium signaling as the readout. The micropipette apparatuses were constructed using a Leica DM IRB inverted microscope placed on an anti-vibration table (Newport) equipped with manometer systems to apply suction pressure through glass pipettes (Supplementary Fig. 8). Two opposing micropipettes mounted on two identical piezoelectric micromanipulators (Sensapex) were used to capture and control the contact between a hexapod and a cell. A sample chamber of the desired size was prepared by cutting coverslips. The temperature of the sample chamber (37 °C) was maintained by an objective heater (Bioptechs). To avoid medium evaporation during heating, the chamber was sealed with mineral oil (Sigma, M8410) on both sides.

For real-time calcium imaging, the sample was illuminated by sequentially triggered exposure to 470 ± 25 nm cyan light or 550 ± 20 nm green light (Spectra X, Lumencor) and a white LED light (TLED+, Sutter Instrument). Triggering of light channels and data acquisition were performed with analog modulation using µManager software (v. 1.4.22)[51]. Time-lapse calcium images were acquired through a ×100 objective by an Andor iXon Ultra EMCCD camera. Signals from calcium dyes were collected at intervals of 500 ms for up to 10–20 min and postprocessed with Fiji software (v.2.3.0) and MATLAB (R2020b). This duration of recording was determined based on our experiences and the literature[7,12,14,52,53].

Single-cell calcium staining

For calcium signaling experiments, ~10^6 cells were incubated with 10 µM calcium indicator ($CD4^+$, $CD8^+$ T cells, Calbryte 520 AM, AAT Bioquest, 20650; CAR-T cells, Calbryte 590 AM, AAT Bioquest, 20700) for 1 hour in HHBS buffer (Hanks' Buffer with 20 mM Hepes) at 37 °C and 5% CO_2 and then incubated at room temperature for 30 min. All imaging experiments were performed in the presence of 2 mM probenecid (Thermo Fisher Scientific, P36400). After incubation, T cells were washed three times with HHBS, resuspended in minimal imaging media (MIM: colorless RPMI with 5% FBS and 10 mM HEPES), incubated in MIM for 10 min at 37 °C and transferred to the micropipette sample chamber before data collection. T cells and hexapods were added to MIM (600 µl) in the homemade cell chamber. Hexapods functionalized with anti-CD3 or CD19 protein were used to investigate TCR or CAR signaling, respectively. The $CD19^+$ NALM-6 B-cell precursor leukemia cell line was used as a positive control.

Rotating magnetic field device

An N52 neodymium permanent magnet (1-inch cube) was attached to a home-built servo-based rotating system (parts obtained from electronics vendor Adafruit, Supplementary Figs. 15 and 18). The rotation speed can be controlled from 0 r.p.m. to 180 r.p.m. The portable devices can be positioned near the cell culture dishes and inside the CO_2 incubator or on the microscope. A three-axis magnetometer was connected to measure the real-time direction and strength of the rotating magnetic field as well as to calibrate the rotation speed. Logfiles and readouts are stored in an SD (secure digital) card. A detailed manual and code of the customized magnet rotator can be accessed via the link https://github.com/MagneticRotor/rotating-magnetic-field.

Magnetic field calculations

Magnetic field $\vec{B}_0$ calculations for the cube magnet were performed using an analytical model[34]. Magnetization was chosen as 1480 mT, a reference value for the N52 magnet (1-inch cubic BX0X0X0-N52, K&J Magnetics). To generate the function of the rotating magnetic field $\vec{B}_{0,\mathrm{rot}}(\vec{v},\theta)$, the z-axis rotation matrix $R_Z(\theta)$ was applied to the static field equation:

$$\vec{B}_0(\vec{v}) = \vec{B}_x(\vec{v}) + \vec{B}_y(\vec{v}) + \vec{B}_z(\vec{v}), \text{where } \vec{v} = \begin{bmatrix} x \\ y \\ z \end{bmatrix}$$

$$R_Z(\theta) = \begin{bmatrix} \cos\theta & -\sin\theta & 0 \\ \sin\theta & \cos\theta & 0 \\ 0 & 0 & 1 \end{bmatrix}$$

$$\vec{B}_{0,\mathrm{rot}}(\vec{v},\theta) = R_Z(\theta)\,\vec{B}_0\left(R_Z(\theta)^{-1}\vec{v}\right)$$

For all plotting, the starting point of rotation was chosen so that the magnetization vector was pointing along the x axis. Calculation and visualization were performed in Wolfram Mathematica (13.0).

Rotation tracking and mean square displacement analysis

To understand the rotational dynamics of the hexapods, we recorded videos of the rotational motion with a Leica DM IRB inverted microscope equipped with a ×100 oil immersion objective (NA 1.40). Naive $CD4^+$ cells (3×10^6 ml^{-1}) were cultured with MCC-hexapods (cell/hexapod ratio, 1:5). Rotation speed was set to 50 r.p.m. and an Andor iXon Ultra EMCCD camera was used for recording (10 frames s^{-1} or 100 ms per frame). Rotational motion was characterized by tracking the center point of the rotating hexapod iron oxide core and the end of one branch tip, or by tracking the center point of hexapod-attached T cells using ImageJ TrackMate. To estimate the MSD, tracking trajectories were analyzed with MATLAB msdanalyzer (https://github.com/tinevez/msdanalyzer) (Supplementary Fig. 17). Diffusion coefficients were calculated based on the first 20% of the MSD curve from the free 2D diffusion equation (MSD = $4\,D \cdot t$).

Co-cultures of rotating hexapods and T or CAR-T cells

To study the impact of biophysical forces on floating primary T cells or CAR-T cells, we set up the rotating magnet device on top of cell culture plates with the help of home-built acrylic holders (Supplementary Fig. 15). Each culture-containing well was the same distance from the magnet. Functionalized hexapods were mixed with T cells or CAR-T cells (1×10^5 cells in 200 µl complete medium per well) with a hexapod/cell ratio of 10:1 and co-cultured for 24 hours. For primary T-cell stimulation, anti-mouse-CD3-hexapods, null-hexapods, MCC-hexapods and OVA-hexapods were used. For CAR-T cell stimulation, CD19-hexapods, BSA-hexapods and anti-human-CD3-hexapods were used. The frequency of the field (optimal rotation speed) was determined to be 30 r.p.m. using optical imaging when the cell's rotation trajectories could be easily tracked.

Cytokine enzyme-linked immunosorbent assay

To measure cell cytokine secretion, supernatants were collected for enzyme-linked immunosorbent assay (ELISA). The supernatant was diluted 1:2 (IL-2) or 1:10 (IFN-γ and TNF-α) with PBS and analyzed using

ELISA MAX Deluxe Set kits according to the manufacturer's instructions (human IL-2, BioLegend, 431804; human IFN-γ, BioLegend, 430104; mouse IL-2, BioLegend, 431004; mouse IFN-γ, BioLegend, 430804; mouse TNF-α, BioLegend, 430904). ELISA plates (Nunc MaxiSorp ELISA Plates, BioLegend, 423501) were read in a microplate spectrophotometer (Epoch, BioTek). For each ELISA, an 8-point standard curve was generated ($R^2 > 0.99$). The raw data were transformed into pg ml^{-1} after fitting to the standard curve.

Cell surface staining and flow cytometry

Following 24 hours of incubation, cell–hexapod pellets obtained by centrifugation were first washed with cold FACS buffer (PBS, 2% BSA, 0.05% sodium azide). Next, Fc receptors were blocked by incubation with Human TruStain FcX (BioLegend, 422302) or Mouse BD Fc Block (clone 2.4G2, BD Pharmingen, 4182991) at 1:50 dilution for 15 min at 4 °C. Cells were incubated for 30 min at 4 °C in the dark with an antibody cocktail (staining solution). The staining solution for $CD4^+$ and $CD8^+$ T cells contained Alexa Fluor 488 anti-mouse CD69 (clone H1.2F3, BioLegend, 104516) and APC anti-mouse CD25 (clone PC61, BioLegend, 102012). Monoclonal antibodies were generally used according to manufacturer recommendations. After staining, cells were incubated briefly with Live/Dead Fixable Near-IR Dead Cell Stain Kit (Invitrogen, L34975), diluted 1:1,000 in PBS, for 30 min at 4 °C in the dark. Cells were washed three times in FACS buffer at 4 °C before analysis by flow cytometry. A total of 50,000 events were acquired on a BD LSRFortessa Cell Analyzer and analysis was performed with the FlowJo software (v10.7.2, BD). The gating strategy is shown in Supplementary Fig. 19.

Single-cell omics assays

OT-1 $CD8^+$ T cells (1%) were added into the wild-type mouse splenocytes repertoire. The cell mixtures were either pretreated with 1 μM TAPI-0 (Sigma, SML1292) (for TNF-α) or incubated with 10 μl IL-2 cytokine catch reagent (Miltenyi Biotec, 130-090-491) (for IL-2). Following two washes, OVA/H-$2K^b$ pMHC-functionalized hexapods were added to the cell mixture and magnetic force was applied. The hexapod–cell mixture was incubated in full culture media with (for TNF-α) or without (for IL-2) 1 μM TAP I-0 in a cell culture incubator maintained at 37 °C and 5% CO_2 to enable the secretion of cytokines.

Following 6 hours of incubation, the hexapod–cell mixture was carefully washed with cold FACS buffer (PBS, 2% BSA, 0.05% sodium azide). Fc receptors were blocked with Mouse TruStain FcX (BioLegend, 156604) at 1:50 dilution for 5 min at 4 °C. Cells were incubated for 30 min at 4 °C in the dark with a staining solution containing BV421-labeled anti-mouse CD45 (clone 30-F11, BioLegend, 103133), BUV395-labeled anti-mouse CD3ε (clone 145-2C11, BD Biosciences, 563565), AF488-labeled anti-mouse CD8α (clone 53-6.7, BioLegend, 100723) or AF488-labeled anti-mouse CD4 (clone RM4-5, BioLegend, 100529), and PE-labeled anti-mouse TNF-α (clone MP6-XT22, BioLegend, 506306) or mouse IL-2 detection antibody (Miltenyi Biotec, 130-090-491) for activated $CD8^+$ or $CD4^+$ T-cell phenotyping and detection. Subsequently, stained cells were conjugated with Live/Dead Fixable Near-IR viability dye (Invitrogen, L34975) at 1:1,000 dilution in PBS for 15 min at 4 °C. Finally, cells were washed three times in cold cell media (RPMI 1640, 10% FBS) before fluorescence-activated cell sorting (BD Biosciences, FACSAria Fusion).

A total of 15,000 sorted cytokine-positive $CD8^+$ T cells ($CD3^+CD8^+IL\text{-}2^+$ or $CD3^+CD8^+TNF\text{-}\alpha^+$) were separately partitioned into droplets for single-cell omics assays using the Chromium Next GEM Single Cell 5′ Kit v2 (10x Genomics, 1000263). RNA-seq libraries were prepared according to manufacturer protocols. TCR-seq libraries were prepared using the Chromium Single Cell Mouse TCR Amplification Kit (10x Genomics, 1000254). All sequencing libraries (RNA-seq, TCR-seq) were quantified via the Qubit dsDNA HS Assay Kit (Invitrogen, Q32851), quality checked for fragment sizes via high-sensitivity D5000 ScreenTapes (Agilent, 5067–5592), pooled, and sequenced (Illumina, NovaSeq 6000).

Joint single-cell RNA-seq and TCR-seq data processing

The cellranger multi pipeline (10x Genomics, version 7.1.0) was used to jointly map and quantify the coupled single-cell RNA-seq (scRNA-seq) and single-cell TCR-seq (scTCR-seq) data for each sample. The reference genome and the TCR pre-assembly reference were all based on mm10 (*Mus musculus*) and provided by 10x Genomics (refdata-gex-mm10-2020A for scRNA-seq; refdata-cellranger-vdj-GRCm38-alts-ensembl-7.0.0 for scTCR-seq). The resultant clonotype and filtered contig annotation data for each sample were used for downstream analyses.

TCR clonotype information for each cell was extracted from the scTCR-seq analyses and matched to the scRNA-seq data for further analyses. Cells in the scRNA-seq data without matched TCR information were categorized as 'NA' for their clonotype and excluded when appropriate from frequency calculation. Cells with the productive target TCRα and TCRβ sequences were categorized as the target antigen-specific cell (for example, for OT-1, Tcra-V2 and Tcrb-V5), and cells with other TCRs were categorized as 'Others'.

Data analysis

Analysis of numerical data and plotting were performed using Microsoft Excel or MATLAB scripts, GraphPad Prism (v.8.4.3), Adobe Illustrator or Wolfram Mathematica (13.0). Codes are available upon request. Statistical analyses were performed in GraphPad Prism (v.8.4.3) using the unpaired two-tailed *t*-test or ANOVA test as indicated in the figure legends.

Data availability

Source data are also provided at https://osf.io/c5y3q/. Sequence data generated in this study are deposited in the National Center for Biotechnology Information Gene Expression Omnibus at https://www.ncbi.nlm.nih.gov/geo/query/acc.cgi?acc=GSE229249. Source data are provided with this paper.

Code availability

The source code for the customized magnet rotator used in this study can be accessed at https://github.com/MagneticRotor/rotating-magnetic-field. Sample codes for analyzing calcium signals using MATLAB and rotation magnetic field simulation using Wolfram Mathematica are available at https://osf.io/c5y3q/. All sequencing analysis was done using standard R packages.

References

50. Kim, J.-H., Hwang, H. J., Oh, J. S., Sacanna, S. & Yi, G.-R. Monodisperse magnetic silica hexapods. *J. Am. Chem. Soc.* **140**, 9230–9235 (2018).
51. Edelstein, A. D. et al. Advanced methods of microscope control using μManager software. *J. Biol. Methods* **1**, e10 (2014).
52. Lee, K., Yi, Y. & Yu, Y. Remote control of T cell activation using magnetic Janus particles. *Angew. Chem. Int. Ed. Engl.* **55**, 7384–7387 (2016).
53. Chen, Y. et al. An integrin αIIbβ3 intermediate affinity state mediates biomechanical platelet aggregation. *Nat. Mater.* **18**, 760–769 (2019).

Acknowledgements

We thank M. Swartz for the generous gift of the OT-1 mice, J. Rowley for the generous gift of the NALM-6 cells, and H. Schreiber for the generous gift of the E6-1 Jurkat cells. We also thank L. Pulido and N. Ankenbruck for general technical assistance, M. Berthoud for technical assistance with the rotating magnetic field device, C. Labno for technical assistance with the FRET experiments, and T.-X. Zheng for providing support on magnetic field calculations. K.M. Watters is thanked for editing the manuscript. We acknowledge start-up grants from the University of Chicago (to B.T. and J.H.), and partial support from the University of Chicago Materials Research

Science and Engineering Center (DMR-2011854; B.T.) and Chicago Immunoengineering Innovation Center (J.H.).

Author contributions

Hexapod synthesis, quantification and characterization: L.M., X.H. and J.S. with input from B.T.; cell culture and cell rotation with hexapods: X.H., L.M., J.Y. and Y.H. with input from J.H.; CAR-T cell construction: Y.H.; T-cell calcium, flow cytometry and ELISA: X.H., M.C. and Y.H.; single-molecule imaging and analysis: X.H. and G.C.; rotation analysis, particle tracking and force estimation: L.M., X.H., A.P. and C.G.; magnetic field calculation and measurement: A.P., L.M. and C.Y.; FRET and 3D imaging: M.C., T.C. and X.H.; identification of antigen-specific TCRs with the hexapod system: X.H. and Y.H.; single-cell sequencing data analysis: G.C.; statistical analysis: L.M. and X.H.; figure preparation and manuscript writing: L.M., X.H., A.P., G.C., M.C., Y.H., T.C. and J.Y. with input from all authors; funding acquisition and supervision: B.T. and J.H. Conception and design of T-cell assays: J.H.

Competing interests

The University of Chicago has filed a provisional patent for the synthesis and application of hexapods for T-cell studies. B.T., J.H., X.H. and L.M. are co-inventors. All other authors have no competing interests.

Additional information

Extended data is available for this paper at https://doi.org/10.1038/s41592-023-02165-7.

Supplementary information The online version contains supplementary material available at https://doi.org/10.1038/s41592-023-02165-7.

Correspondence and requests for materials should be addressed to Jun Huang or Bozhi Tian.

Peer review information *Nature Methods* thanks Cheng Zhu and the other, anonymous, reviewer(s) for their contribution to the peer review of this work. Primary Handling Editor: Madhura Mukhopadhyay, in collaboration with the *Nature Methods* team.